

Comparison of acute thrombogenicity for magnesium versus stainless steel stents in a porcine arteriovenous shunt model



Michael J. Lipinski¹, MD, PhD; Eduardo Acampado², DVM; Qi Cheng², MD; Lila Adams², AS; Sho Torii², MD; Jiaxiang Gai¹, MSPH; Rebecca Torguson¹, MPH; David G. Hellinga¹, MSc; Michael Joner³, MD; Claus Harder⁴, PhD; Philine Zumstein⁴, BSBT; Alope Finn², MD, PhD; Frank D. Kolodgie², PhD; Renu Virmani², MD; Ron Waksman^{1*}, MD

1. Section of Interventional Cardiology, MedStar Washington Hospital Center, Washington, DC, USA; 2. CVPPath Institute Inc., Gaithersburg, MD, USA; 3. Deutsches Herzzentrum München, Technische Universität München, Munich, Germany; 4. Biotronik AG, Bülach, Switzerland

KEYWORDS

- bioresorbable scaffolds
- drug-eluting stent

Abstract

Aims: The present study aimed to investigate whether the Magmaris resorbable magnesium scaffold (RMS) has platelet-repelling properties by comparing its acute thrombogenicity with an equivalent stainless steel stent in an arteriovenous shunt model.

Methods and results: An *ex vivo* porcine carotid jugular arteriovenous shunt was established and connected to Sylgard tubing containing the Magmaris RMS with sirolimus-eluting PLLA coating and an equivalent 316L stainless steel stent with sirolimus-eluting PLLA coating. Six shunts (two shunt runs per pig) were run comparing the two scaffolds (n=9) in alternating order. Nested generalised linear mixed models were employed to compare variables between scaffold groups. Confocal fluorescent microscopy containing CD61/CD42b demonstrated that the 316L equivalent stent had significantly greater platelet coverage of the total scaffold compared with Magmaris (5.8% vs. 2.8%, adjusted rate ratio 2.21 [1.41, 3.47], p=0.012). Scanning electron microscopy demonstrated significantly greater thrombus deposition on the 316L equivalent stent as a percentage of the total scaffold compared with Magmaris (8.0% vs. 5.3%, p=0.009). Magmaris also had significantly less CD14 positive monocyte deposition and a trend towards less PM-1 positive neutrophil compared with the 316L equivalent stent.

Conclusions: Magmaris has less thrombogenicity and inflammatory cell deposition compared with the equivalent 316L stainless steel (in geometry and design) stent in a porcine arteriovenous shunt model. These data suggest that resorbable magnesium scaffolds may have inherent properties that reduce adhesion of platelets and inflammatory cells.

*Corresponding author: MedStar Heart and Vascular Institute, MedStar Washington Hospital Center, 110 Irving St, NW, Suite 4B-1, Washington, DC 20010, USA. E-mail: ron.waksman@medstar.net

Abbreviations

| | |
|-------------|---------------------------------|
| BVS | bioresorbable vascular scaffold |
| DES | drug-eluting stent |
| PLLA | poly-L-lactic acid |
| RMS | resorbable magnesium scaffold |
| SEM | scanning electron microscopy |

Introduction

Scaffold thrombosis has emerged as a major concern in bioresorbable scaffold technology¹. In addition to clinical studies demonstrating a higher incidence of scaffold thrombosis with the Absorb bioresorbable vascular scaffold (BVS) (Abbott Vascular, Santa Clara, CA, USA) compared with second-generation drug-eluting stents (DES)^{2,3}, we recently demonstrated that the Absorb BVS has greater acute thrombogenicity and deposition of inflammatory cells compared with the Magmaris resorbable magnesium scaffold (RMS) (Biotronik AG, Bülach, Switzerland)⁴. Interestingly, the Magmaris also had comparable or even slightly reduced thrombogenicity compared with the Orsiro hybrid DES (Biotronik AG)⁴, which has significantly thinner struts but an identical sirolimus-eluting bioresorbable poly-L-lactic acid (PLLA) coating. These data raise the question whether the magnesium stent backbone has inherent properties that may reduce adhesion of platelets and leukocytes.

While previous studies have suggested that magnesium stents were free of thrombosis in clinical trials⁵ and may have reduced thrombogenicity compared with other metallic stents, there remain differences between the stents, such as strut thickness, strut shape, stent coating, and stent design, that may account for differences in fluid dynamics and platelet deposition. Therefore, we generated a 316L stainless steel stent with sirolimus-eluting PLLA coating (316L equivalent stent; Biotronik AG) identical to the Magmaris RMS, which differs only in the composition of the stent backbone, to enable a true comparison of whether magnesium has inherent properties that reduce platelet and leukocyte deposition. We sought to compare the acute thrombogenicity of the Magmaris RMS with the 316L equivalent stent in an established porcine *ex vivo* carotid jugular arteriovenous shunt model.

Methods

ETHICS STATEMENT

Animal handling and care followed the recommendations of the National Institutes of Health Guide for the Care and Use of Laboratory Animals. All protocols were approved by the Animal Care and Use Committee at MedStar Washington Hospital Center, Washington, DC, USA.

EXPERIMENTAL SET-UP AND TEST GROUPS

The Magmaris resorbable magnesium scaffold has a sirolimus-eluting bioresorbable PLLA coating with a sirolimus load of 1.4 µg/mm². We generated an equivalent 316L stainless steel stent with a sirolimus-eluting bioresorbable PLLA coating with a sirolimus load

of 1.4 µg/mm² (316L equivalent stent). Both stents had identical dimensions of 3.0x20 mm, 150 µm strut thickness and width, and an identical stent design. A porcine *ex vivo* arteriovenous shunt model was established to study the extent of platelet adherence, thrombus formation, and acute inflammation for the Magmaris (n=9) and 316L equivalent stent (n=9).

The Magmaris and 316L equivalent stents were deployed in alternating order in each shunt model, and two shunt experiments were conducted for each animal. Each shunt included three stents in which we alternated the order of Magmaris and 316L equivalent stents, resulting in three shunts containing two Magmaris on either side of one 316L equivalent stent and three shunts containing two 316L equivalent stents on either side of one Magmaris. Thus, a total of 18 scaffolds/stents were studied (nine per group) using six shunt runs in three swine.

PORCINE ARTERIOVENOUS SHUNT MODEL

Silicone elastomer tubes were generated from Sylgard® 184 (Dow Corning, Midland, MI, USA) to have an inner diameter of 2.70 mm and total length of 11 cm using an established protocol⁶. Coronary scaffolds/stents were deployed within the tubing based on the manufacturer's suggested nominal pressure (Magmaris at 10 atmospheres; 316L equivalent stent at 12 atmospheres) to obtain a stent to Sylgard tube ratio of 1.1:1.0. The tubing was initially primed with autologous platelet-poor plasma, and the distance between scaffolds/stents was maintained at 1.0 cm.

Yorkshire cross domestic pigs were anaesthetised with ketamine/xylazine, intubated, and maintained on isoflurane throughout the procedure. Following surgical cut-down, the carotid artery and internal jugular vein were cannulated with 9 Fr vascular sheaths, the haemostatic valves from the sheaths were cut off, and the remaining stem was attached to TYGON® Silicone Tubing (Cole-Parmer, Vernon Hills, IL, USA), which was then connected to the proximal and distal Luer fittings affixed to the Sylgard tubing containing the scaffold/stents, which was kept in a 37°C water bath (model #W2M; Sheldon Manufacturing, Inc., Cornelius, OR, USA). The flow rate through the loop was monitored continuously using an ultrasonic flow transducer (Transonic, Ithaca, NY, USA) (Figure 1, upper panel). After establishing vascular access, unfractionated heparin was administered intravenously to achieve target activated clotting times (ACT) of between 150 and 200 seconds prior to initiation of the shunt runs without antiplatelet agents such as aspirin or clopidogrel, as the study was specifically designed to assess platelet-mediated thrombus formation induced by the scaffold/stents.

SAMPLE FIXATION

After 60 minutes of continuous blood flow or reduction of blood flow by 50% as measured by the ultrasonic transducer, the circuit was interrupted and the TYGON tubing was disconnected from the Sylgard shunt tubing. The stents were then gravity perfused with 250 mL of Ringer's lactate solution followed by 10% neutral buffered formalin. The most proximal end of the shunt

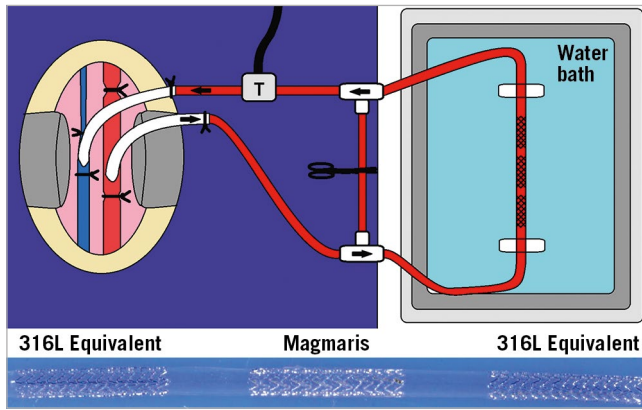


Figure 1. Shunt cartoon with representative shunt. Cartoon (upper panel) illustrating the ex vivo porcine carotid jugular arteriovenous shunt model. Arterial blood flows from the carotid artery into the vascular sheath, through the TYGON tubing, passes through the Sylgard shunt tubing containing the scaffolds/stents, back into the TYGON tubing, through the ultrasonic transducer (T) which measures blood flow, and the blood flows back into the internal jugular vein. The arrows show the direction of blood flow. The lower panel shows a representative shunt with the scaffolds/stents within the Sylgard shunt tubing with labels for the respective scaffolds/stents.

(arterial side) was cut at an angle for orientation and the stents were then immersion-fixed in formalin for 20 minutes at room temperature, rinsed in phosphate buffered saline (PBS), and kept in 15% sucrose weight/volume diluted in PBS without Ca²⁺/Mg⁺ with a pH of 7.4-7.6 at 4°C until immunolabelling for platelets and inflammatory cells.

ASSESSMENT OF PLATELET AND INFLAMMATORY CELL ADHESION BY CONFOCAL MICROSCOPY

After fixation, the stents were photographed and then carefully removed from the Sylgard tubing. Each stent was bisected longitudinally to expose the luminal surface. Both halves of the stent were immunostained for adherent platelets using an antibody cocktail directed against platelet-specific markers CD61 and CD42b and subsequently with antibodies targeting the neutrophil marker PM-1 and monocyte marker CD14, as previously described⁴.

Confocal microscopy was performed as previously described⁴. As both the Magmaris and the 316L equivalent stent have 11 struts, we measured strut numbers 1, 3, 5, 7, 9, and 11 (each strut [n=6] had a 20x high-power image). Images for quantification of inflammatory cells were acquired at every other strut for both the Magmaris and the 316L equivalent stent, as previously described⁴.

SCANNING ELECTRON MICROSCOPY

The second half of the scaffold/stent was processed for scanning electron microscopy (SEM) where specimens were dehydrated, critically point dried, and sputter-coated with gold. SEM was performed as previously described⁴.

BLOOD COAGULATION AND PLATELET FUNCTION TESTS

Blood was serially drawn pre-shunt (baseline) and after each experimental run to confirm the degree of anticoagulation. Platelet count, prothrombin time, and partial thromboplastin time were performed by our clinical lab.

STATISTICAL ANALYSIS

Statistical analyses were performed using SAS 9.2 (SAS Institute, Cary, NC, USA). Continuous variables are presented as mean±standard deviation in the case of normal distribution or median with interquartile range (IQR) in the case of non-normal distribution. Nested generalised linear mixed models (GLMM) were employed in order to investigate group differences in consideration of multiple measurements per individual shunt. Within these models, the experimental factor variables animal, shunt number, scaffold position, and partial thromboplastin time value were considered as nested random effects. To adjust for non-constant variance, we performed log transformation. The Akaike information criterion (AIC) was evaluated for the goodness of model fit, and only the number of cell nuclei on the stent surface was logarithmically transformed prior to analysis. The Bonferroni method was used to adjust for multiple comparisons to implement adjustment of p-values and confidence interval lengths for multiple testing. Data for comparison between stent/scaffold groups are presented as rate ratio (95% confidence intervals [CI]). A p-value ≤0.05 was considered statistically significant, and two-tailed tests were utilised.

Results

BLOOD COAGULATION AND PLATELET FUNCTION

During the six shunt runs, the mean ACT value was 153±6 seconds with a range from 149 to 165 seconds. Individual readings below 150 seconds and above 200 seconds were adjusted by administering heparin or holding heparin, respectively. The mean blood-flow rate through the shunt circuit during the shunt runs was 139±6 mL/minute with a range of 131 to 148 mL/minute. All shunts ran the entire 60 minutes as planned. The platelet count, prothrombin time, and partial thromboplastin time at baseline, after the first shunt run, and after the second shunt run for each animal can be found in **Table 1**.

Table 1. Platelet and coagulation levels from the pigs prior to anticoagulation (baseline), and after completion of the 1st shunt run and 2nd shunt run in each animal. All three values are presented for each shunt run.

| | Baseline | After 1 st shunt | After 2 nd shunt |
|---------------------------------------|-----------------|-----------------------------|-----------------------------|
| Platelet count (×1,000/μL) | 264, 228, 202 | 228, 166, 230 | 202, 165, 190 |
| Prothrombin time (seconds) | 9.1, 9.3, 8.8 | 9.6, 10.2, 10.7 | 10.1, 10.2, 11.8 |
| Partial thromboplastin time (seconds) | 12.6, 10.9, 9.7 | 11.5, 23.6, >100 | 28.3, 36.5, >100 |

ACUTE THROMBOGENICITY ASSESSED BY PLATELET IMMUNOFLUORESCENCE

At the time of processing, all stents were assessed for adequate strut apposition. There was no evidence of malapposition as all struts were adequately apposed with the Sylgard shunt tubing. Visual assessment of the stents following the shunt runs did not demonstrate an obvious difference in thrombus deposition between the Magmaris and 316L equivalent stents (Figure 1, lower panel). However, visual assessment of the Magmaris and 316L equivalent stents on confocal microscopy co-staining for CD42b/CD61 appeared to demonstrate greater platelet deposition on the 316L equivalent stents compared with the Magmaris (Figure 2A). Confocal microscopy for CD42b/CD61 staining as percentage of the total scaffold surface area demonstrated significantly greater platelet deposition for the 316L equivalent stent (5.82% [range 3.89-8.0%]) compared with the Magmaris (2.84% [range 1.98-3.37%], adjusted rate ratio 2.21 [95% CI: 1.41, 3.47], $p=0.012$) (Figure 2B, Table 2, Table 3). When assessing the percentage of strut coverage by CD42b/CD61 positive platelets (Figure 2C, Table 2, Table 3), the 316L equivalent stent (25.8% [range 16.1-36.0%]) had significantly greater coverage compared with the Magmaris (12.5% [range 8.3-16.6%], adjusted rate ratio 2.12 [95% CI: 1.21, 3.70], $p=0.023$).

Table 2. Medians with interquartile range (IQR) of percent CD42b/CD61 fluorescence positive of total scaffold surface area, percent CD42b/CD61 fluorescence positive of total scaffold strut area, percent thrombus coverage of the total scaffold, neutrophil cell density on the scaffold struts, and monocyte cell density on the scaffold struts by confocal microscopy and scanning electron microscopy (SEM) between Magmaris and 316L equivalent stent in an *ex vivo* porcine arteriovenous shunt model.

| | Magmaris | 316L equivalent stent |
|---|--------------------|-----------------------|
| Percent CD42b/CD61 fluorescence positive of total scaffold surface area, % | 2.84 [1.98-3.37] | 5.82 [3.89-8.00] |
| Percent CD42b/CD61 fluorescence positive of total scaffold strut area, % | 12.52 [8.27-16.55] | 25.77 [16.13-36.0] |
| Percent thrombus coverage of the total scaffold by SEM, % | 5.33 [5.0-5.67] | 8.0 [7.0-13.67] |
| Neutrophil cell density on the scaffold struts (PM-1 positive cells/mm ²) | 31 [20-79] | 243 [30-357] |
| Monocyte cell density on the scaffold struts (CD14 positive cells/mm ²) | 40 [24-88] | 168 [99-351] |

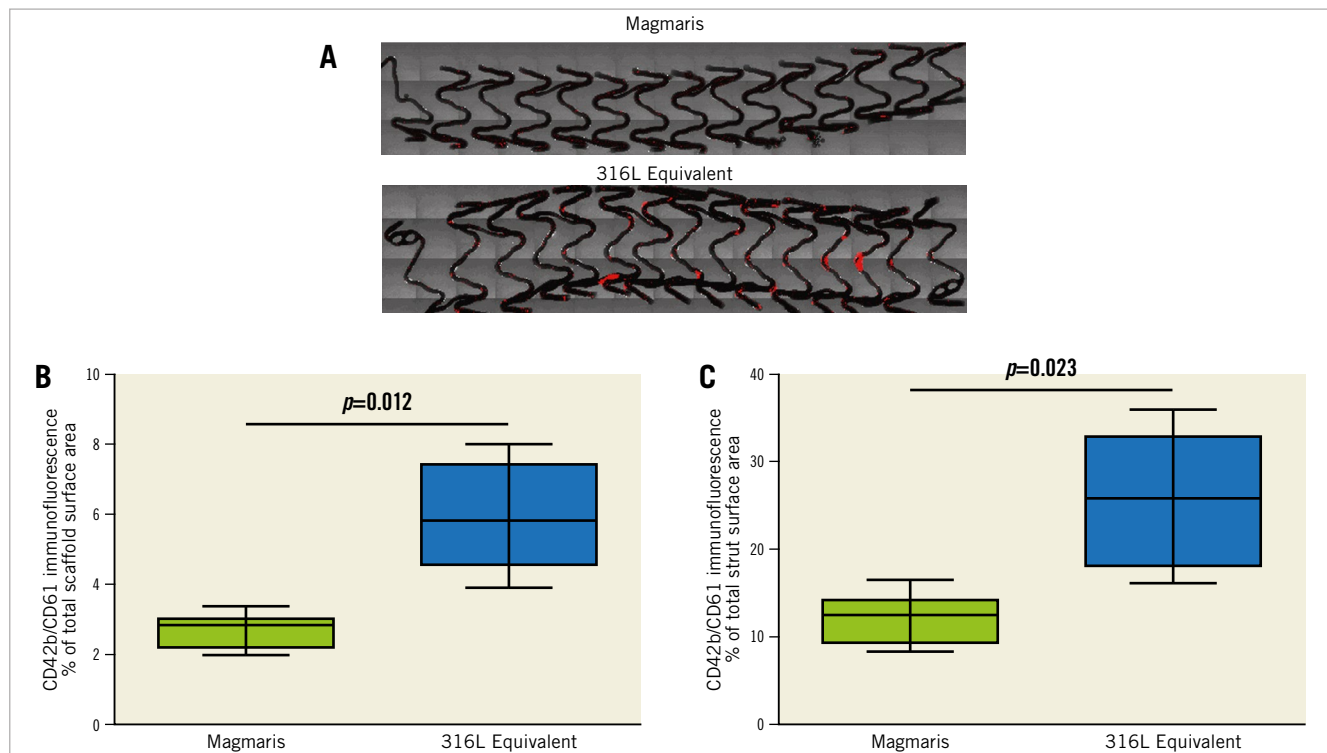


Figure 2. Comparison of platelet adhesion to the Magmaris and a 316L stainless steel equivalent stent from confocal microscopy with immunofluorescent staining against dual platelet markers (CD61/CD42b) in a swine shunt model. Representative confocal microscopy images (A) of Magmaris and a 316L equivalent stent are provided with dual staining for platelet markers CD42b/CD61 (red channel, 555 nm). Comparisons of CD42b/CD61 immunofluorescence as a percentage of the total scaffold area (B) and as a percentage of the total strut area (C) are provided for the Magmaris and a 316L equivalent stent. Data are presented as box plots demonstrating the median and quartiles with whiskers representing the minimum and maximum values for each group and p -values comparing between the groups based on nested generalised linear mixed models to adjust for variations between the shunt runs present in Table 3.

Table 3. Adjusted rate ratios (95% CI) based on nested generalised linear mixed models for comparisons of percent CD42b/CD61 fluorescence positive of total scaffold surface area, percent CD42b/CD61 fluorescence positive of total scaffold strut area, percent thrombus coverage of the total scaffold, neutrophil cell density on the scaffold struts, and monocyte cell density on the scaffold struts by confocal microscopy and scanning electron microscopy (SEM) between 316L equivalent stent vs. Magmaris in an *ex vivo* porcine arteriovenous shunt model.

| | Rate ratio (95% CI) | p-value |
|---|---------------------|---------|
| Percent CD42b/CD61 fluorescence positive of total scaffold surface area, % | | |
| 316L equivalent stent vs. Magmaris | 2.21 (1.41, 3.47) | 0.012 |
| Percent CD42b/CD61 fluorescence positive of total strut area, % | | |
| 316L equivalent stent vs. Magmaris | 2.12 (1.21, 3.70) | 0.023 |
| Percent thrombus coverage of the total scaffold by SEM, % | | |
| 316L equivalent stent vs. Magmaris | 1.65 (1.26, 2.16) | 0.009 |
| Neutrophil cell density on the scaffold struts (PM-1 positive cells/mm ²) | | |
| 316L equivalent stent vs. Magmaris | 5.04 (0.72, 35.45) | 0.078 |
| Monocyte cell density on the scaffold struts (CD14 positive cells/mm ²) | | |
| 316L equivalent stent vs. Magmaris | 4.73 (2.15, 10.42) | 0.008 |
| A rate ratio >1 denotes greater levels of the parameter in the 316L equivalent stent compared with the Magmaris. A rate ratio <1 denotes lower levels of the parameter in the 316L equivalent stent compared with the Magmaris. SEM: scanning electron microscopy | | |

THROMBUS DEPOSITION AND INFLAMMATORY CELL ADHERENCE ASSESSED BY SCANNING ELECTRON MICROSCOPY

SEM was performed for further quantification of thrombus deposition on the scaffold/stents. Representative examples of SEM images for the Magmaris and the 316L equivalent stent can be found in **Figure 3A**. Quantification of thrombus deposition on the scaffolds as a measure of percentage of the total surface area demonstrated that the 316L equivalent stent had significantly greater thrombus deposition than the Magmaris (8.0% vs. 5.3%, respectively, adjusted rate ratio 1.65 [95% CI: 1.26, 2.16], p=0.009) (**Figure 3B, Table 2, Table 3**).

INFLAMMATORY CELL DEPOSITION ASSESSED BY CONFOCAL MICROSCOPY

To assess for the presence of inflammatory cells on the scaffolds/stents, confocal microscopy was performed to assess for the presence of neutrophils and monocytes. Representative confocal microscopy images appeared to demonstrate fewer PM-1 positive neutrophils on the Magmaris than the 316L equivalent stents (**Figure 4A**). Similarly, representative confocal microscopy images appeared to demonstrate fewer CD14 positive monocytes on the Magmaris than the 316L equivalent stents (**Figure 4B**). When performing quantitative analysis, confocal microscopy for PM-1 positive cells demonstrated a trend towards greater neutrophil adherence to the 316L equivalent stent (243 cells/mm² [range 30-357]) compared with the Magmaris (31 cells/mm² [range

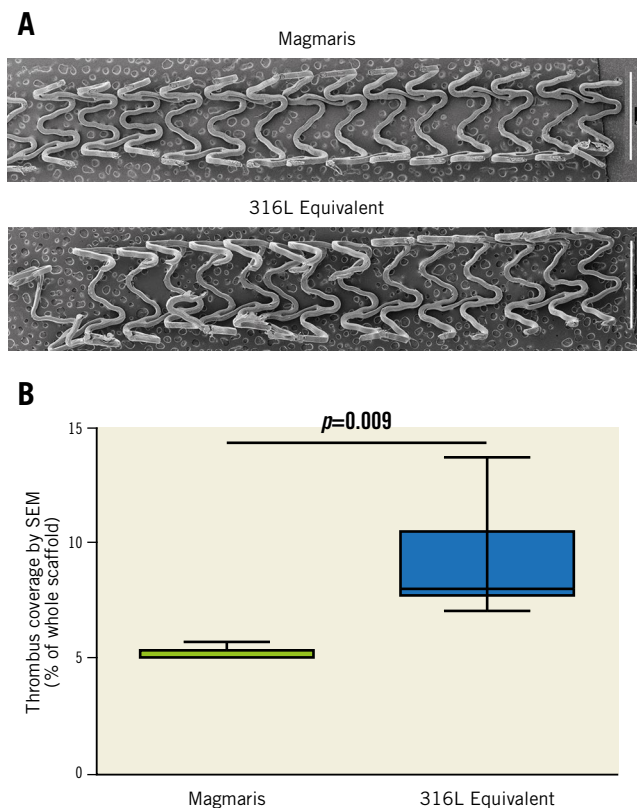


Figure 3. Scanning electron microscopy (SEM) images comparing thrombus formation on the Magmaris and a 316L stainless steel equivalent stent. Representative low-power SEM images (A) of the Magmaris and a 316L equivalent stent following a one-hour shunt run in the porcine *ex vivo* arteriovenous shunt model. Stitched montage images (x15 magnification) of the entire luminal surface were assembled into a single image. Comparison of thrombus deposition as a percentage of the total scaffold area (B) is provided for the Magmaris and a 316L equivalent stent. Data are presented as box plots demonstrating the median and quartiles with whiskers representing the minimum and maximum values for each group and p-value comparing between the groups based on nested generalised linear mixed models to adjust for variations between the shunt runs present in Table 3.

20-79], adjusted rate ratio 5.04 [95% CI: 0.72, 35.45], p=0.078) (**Figure 4C, Table 2, Table 3**). Confocal microscopy for CD14 positive cells demonstrated significantly greater monocyte adherence to the 316L equivalent stent (168 cells/mm² [range 99-351]) compared with the Magmaris (40 cells/mm² [IQR 24-88], adjusted rate ratio 4.73 [95% CI: 2.15, 10.42], p=0.008) (**Figure 4D, Table 2, Table 3**).

Discussion

This study compared the acute thrombogenicity of the Magmaris RMS with an equivalent 316L stainless steel stent using an *ex vivo* porcine arteriovenous shunt model by assessing platelet and inflammatory cell adhesion to the scaffolds/stents. The study demonstrated that the Magmaris had significantly less platelet

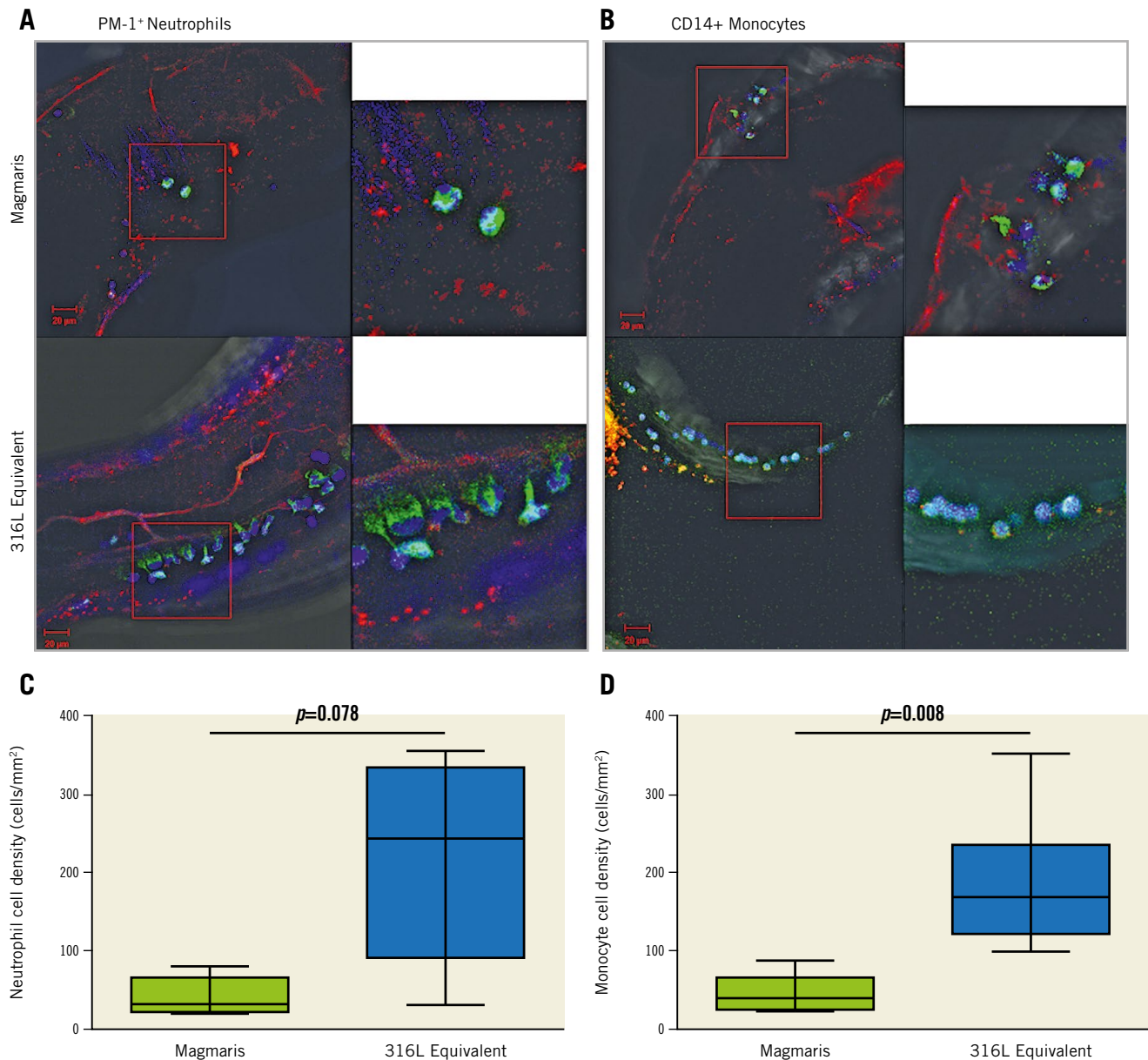


Figure 4. Comparison of inflammatory cell adherence to the Magmaris and a 316L stainless steel equivalent stent from confocal microscopy with immunofluorescent staining against neutrophils (PM-1) and monocytes (CD14) in a swine shunt model. Representative confocal microscopy images of the Magmaris and a 316L equivalent stent are provided with dual staining for platelet markers CD42b/CD61 (red channel, 555 nm) with panels to the left staining PM-1 positive neutrophils (A) (green channel, 488 nm) and panels to the right staining CD14 positive monocytes (B) (green channel, 488 nm). Nuclei are counterstained with DAPI (blue channel). Comparison of neutrophil cell density (PM-1 positive cells/mm²) (C) and monocyte cell density (CD14 positive cells/mm²) (D) are provided for the Magmaris and a 316L equivalent stent. Data are presented as box plots demonstrating the median and quartiles with whiskers representing the minimum and maximum values for each group and p-values comparing between the groups based on nested generalised linear mixed models to adjust for variations between the shunt runs present in Table 3.

adherence, thrombus deposition, and monocyte adherence as well as a trend towards less neutrophil adherence compared with a 316L equivalent stent. It is critical to note that these stents have the same design, the same sirolimus-eluting PLLA coating and the same strut thickness, and only differ in the stent backbone. Thus, our study suggests that the magnesium backbone may have inherent properties that reduce adhesion of platelets and inflammatory

leukocytes compared with an equivalent stainless steel stent, despite having an identical sirolimus-eluting PLLA coating.

Stents composed of different metal alloys have been studied extensively to assess inherent thrombogenicity, but many of these studies are limited due to small differences in stent design, strut shape, etc. There are also clear differences between the use of arteriovenous shunt models and other *in vitro* systems such as Chandler

loops. When assessed in Chandler loops, magnesium stents were shown to have negligible thrombogenic properties when interacting with whole blood for 90 or 360 minutes⁷. Platelet deposition and thrombus activation were also reduced with magnesium stents compared with both uncoated stainless steel and cobalt-chromium alloy stents⁸. This may occur because magnesium stents are negatively charged⁹, which may help to repel negatively charged platelets and minimise thrombogenicity¹⁰. It is important to note that magnesium stents experience rapid onset of corrosion, which is the mechanism by which resorbable magnesium scaffolds break down⁷.

The polymeric coating of RMS may help to delay degradation but was also found to reduce platelet adherence and thrombogenicity further^{11,12}. Interestingly, biodegradable polymer coating was shown to have evidence of cracking early after deployment in a rabbit iliofemoral stent model¹³. The Magmaris scaffold was also compared with the Absorb BVS and found to have superior endothelialisation and decreased thrombus formation at three and 28 days in preclinical animal studies¹⁴. This study builds on our earlier study, which demonstrated that the Magmaris had significantly less platelet deposition and thrombus formation along with less inflammatory cell deposition than the Absorb BVS⁴. It is important to note that the Magmaris RMS and Absorb BVS have a similar strut thickness of 150 µm, though the strut width for Absorb BVS may be as high as 197 µm¹⁵. Additionally, the degree of platelet deposition and thrombus formation on the Magmaris is nearly identical to that seen in our previous study⁴, highlighting the reproducibility of this model. Despite a favourable safety profile for the Magmaris in the initial first-in-man study⁵, further preclinical and clinical studies are needed.

Limitations

The main limitation of this study is its *ex vivo* design. Though artificial, the *ex vivo* arteriovenous porcine shunt model has been shown to be very consistent and reproducible, while scaffold deployment in the coronary arteries is highly variable with differences in vessel diameter, the presence of side branches, which coronary artery is stented (left anterior descending, left circumflex, right), etc. The findings of this study are consistent with prior data for the Magmaris employing this model⁴. We did not assess how porous the polymer coating is for the stents and whether Mg²⁺ ions are released, nor did we assess the rapidity of corrosion in these studies. The comparison of the Magmaris with a 316L equivalent stent further aids in reducing variability. However, a Magmaris RMS without a polymer coating could have served as an additional control. Another limitation is that the flow velocity of blood through the shunt is different from that of the coronary arteries, raising the question whether this may modulate platelet activation. Additional studies confirming our findings utilising an *in vivo* model or alternative *ex vivo* or *in vitro* models to assess acute thrombogenicity, such as a Badimon chamber^{16,17} or Chandler Loop Apparatus^{18,19}, would add to the strength of our findings. Finally, another major limitation is the

lack of antiplatelet therapy such as a P2Y₁₂ inhibitor. However, studying such phenomena as in the present study is best performed without interfering with their function, i.e., without antiplatelet therapy.

Conclusions

In conclusion, the Magmaris sirolimus-eluting RMS had reduced acute thrombogenicity compared with an equivalent 316L stainless steel stent despite having the same sirolimus-eluting coating. Thus, our data suggest that resorbable magnesium scaffolds may have inherent properties that reduce adhesion of platelets and inflammatory cells.

Impact on daily practice

The current preclinical data demonstrate that the Magmaris resorbable magnesium scaffold (RMS) with sirolimus-eluting coating has significantly less acute thrombogenicity than an equivalent sirolimus-eluting 316L stainless steel stent. This implies that the magnesium-based Magmaris RMS may have inherent platelet-repelling properties that may reduce the risk of scaffold thrombosis. Further randomised controlled trials are necessary to determine whether the Magmaris RMS has a reduced risk of scaffold thrombosis compared with contemporary drug-eluting stents.

Funding

The source of funding for this research was Biotronik AG.

Conflict of interest statement

R. Waksman is a consultant for and has received grant support (significant) from Biotronik and Biosensors International. M. Joner is a consultant (modest) for Biotronik and OrbusNeich, and has received speaker honoraria (modest) from Biotronik, Boston Scientific, Abbott Vascular, OrbusNeich, and AstraZeneca. P. Zumstein and C. Harder are employees (significant) of Biotronik. R. Virmani declares research support (all significant) from Abbott Vascular, Biosensors International, Biotronik, Boston Scientific, Medtronic, MicroPort Medical, OrbusNeich Medical, SINO Medical Technology, and Terumo Corporation; speaking engagements (significant) with Merck; honoraria (all significant) from Abbott Vascular, Boston Scientific, Lutonix, Medtronic, and Terumo Corporation; and being a consultant (all significant) for Biomedical, Abbott Vascular, Medtronic, and W.L. Gore. The other authors have no conflicts of interest to declare.

References

1. Capodanno D, Joner M, Zimarino M. What about the risk of thrombosis with bioresorbable scaffolds? *EuroIntervention*. 2015;11 Suppl V:V181-4.
2. Lipinski MJ, Escarcega RO, Baker NC, Benn HA, Gaglia MA Jr, Torguson R, Waksman R. Scaffold Thrombosis After Percutaneous Coronary Intervention With ABSORB Bioresorbable

Vascular Scaffold: A Systematic Review and Meta-Analysis. *JACC Cardiovasc Interv.* 2016;9:12-24.

3. Ali ZA, Serruys PW, Kimura T, Gao R, Ellis SG, Kereiakes DJ, Onuma Y, Simonton C, Zhang Z, Stone GW. 2-year outcomes with the Absorb bioresorbable scaffold for treatment of coronary artery disease: a systematic review and meta-analysis of seven randomised trials with an individual patient data substudy. *Lancet.* 2017;390:760-72.

4. Waksman R, Lipinski MJ, Acampado E, Cheng Q, Adams L, Torii S, Gai J, Torguson R, Hellinga DM, Westman PC, Joner M, Zumstein P, Kolodgie FD, Virmani R. Comparison of Acute Thrombogenicity for Metallic and Polymeric Bioabsorbable Scaffolds: Magmaris Versus Absorb in a Porcine Arteriovenous Shunt Model. *Circ Cardiovasc Interv.* 2017 Aug;10(8).

5. Haude M, Ince H, Abizaïd A, Toelg R, Lemos PA, von Birgelen C, Christiansen EH, Wijns W, Neumann FJ, Kaiser C, Eeckhout E, Lim ST, Escaned J, Garcia-Garcia HM, Waksman R. Safety and performance of the second-generation drug-eluting absorbable metal scaffold in patients with de-novo coronary artery lesions (BIOSOLVE-II): 6 month results of a prospective, multi-centre, non-randomised, first-in-man trial. *Lancet.* 2016;387:31-9.

6. Colombo A, Zahedmanesh H, Toner DM, Cahill PA, Lally C. A method to develop mock arteries suitable for cell seeding and in-vitro cell culture experiments. *J Mech Behav Biomed Mater.* 2010;3:470-7.

7. Feyerabend F, Wendel HP, Mihailova B, Heidrich S, Agha NA, Bismayer U, Willumeit-Römer R. Blood compatibility of magnesium and its alloys. *Acta Biomater.* 2015;25:384-94.

8. Hansi C, Arab A, Rzany A, Ahrens I, Bode C, Hehrlein C. Differences of platelet adhesion and thrombus activation on amorphous silicon carbide, magnesium alloy, stainless steel, and cobalt chromium stent surfaces. *Catheter Cardiovasc Interv.* 2009;73:488-96.

9. Sawyer PN, Srinivasan S. The role of electrochemical surface properties in thrombosis at vascular interfaces: cumulative experience of studies in animals and man. *Bull N Y Acad Med.* 1972;48:235-56.

10. Sarkar S, Sales KM, Hamilton G, Seifalian AM. Addressing thrombogenicity in vascular graft construction. *J Biomed Mater Res B Appl Biomater.* 2007;82:100-8.

11. Gu X, Mao Z, Ye SH, Koo Y, Yun Y, Tiasha TR, Shanov V, Wagner WR. Biodegradable, elastomeric coatings with controlled anti-proliferative agent release for magnesium-based cardiovascular stents. *Colloids Surf B Biointerfaces.* 2016;144:170-9.

12. Ye SH, Jang YS, Yun YH, Shankarraman V, Woolley JR, Hong Y, Gamble LJ, Ishihara K, Wagner WR. Surface modification of a biodegradable magnesium alloy with phosphorylcholine (PC) and sulfobetaine (SB) functional macromolecules for reduced thrombogenicity and acute corrosion resistance. *Langmuir.* 2013;29:8320-7.

13. Yazdani SK, Sheehy A, Pacetti S, Rittlemeier B, Kolodgie FD, Virmani R. Stent Coating Integrity of Durable and Biodegradable Coated Drug Eluting Stents. *J Interv Cardiol.* 2016;29:483-90.

14. Waksman R, Zumstein P, Pritsch M, Wittchow E, Haude M, Lapointe-Corriveau C, Leclerc G, Joner M. Second-generation magnesium scaffold Magmaris: device design and preclinical evaluation in a porcine coronary artery model. *EuroIntervention.* 2017;13:440-9.

15. Ormiston JA, Webber B, Ubod B, Darremont O, Webster MW. An independent bench comparison of two bioresorbable drug-eluting coronary scaffolds (Absorb and DESolve) with a durable metallic drug-eluting stent (ML8/Xpedition). *EuroIntervention.* 2015;11:60-7.

16. Fuster V, Ip JH, Badimon L, Badimon JJ, Stein B, Chesebro JH. Importance of experimental models for the development of clinical trials on thromboatherosclerosis. *Circulation.* 1991;83:IV15-25.

17. Lucking AJ, Chelliah R, Trotman AD, Connolly TM, Feuerstein GZ, Fox KA, Boon NA, Badimon JJ, Newby DE. Characterisation and reproducibility of a human ex vivo model of thrombosis. *Thromb Res.* 2010;126:431-5.

18. Chin-Quee SL, Hsu SH, Nguyen-Ehrenreich KL, Tai JT, Abraham GM, Pacetti SD, Chan YF, Nakazawa G, Kolodgie FD, Virmani R, Ding NN, Coleman LA. Endothelial cell recovery, acute thrombogenicity, and monocyte adhesion and activation on fluorinated copolymer and phosphorylcholine polymer stent coatings. *Biomaterials.* 2010;31:648-57.

19. Tepe G, Schmehl J, Wendel HP, Schaffner S, Heller S, Gianotti M, Claussen CD, Duda SH. Reduced thrombogenicity of nitinol stents--in vitro evaluation of different surface modifications and coatings. *Biomaterials.* 2006;27:643-50.